

# A Jet Noise Prediction Model for Chevrons and Microjets

N.K. Depuru Mohan\* and A.P. Dowling†

*Department of Engineering, University of Cambridge, Cambridge CB2 1PZ, UK*

This study develops a jet noise prediction model for chevrons and microjets. A novel equation is proposed to express the amplitude of the fourth-order space-time velocity cross-correlations, which represent the sources of noise emanated from unheated jets, in terms of mean flow parameters and turbulence statistics such as streamwise circulation, axial velocity and turbulent kinetic energy. The cross-correlations based on a Reynolds Averaged Navier-Stokes (RANS) flowfield showed a good agreement with those based on a Large Eddy Simulation (LES) flowfield. With the novel acoustic source description, there is a good agreement between the model's jet noise predictions and the experimental data for unheated jets for a wide range of frequencies and observer angles for both chevrons and microjets.

As the model provides quick and accurate jet noise predictions, a parametric study is performed to understand the impact of chevrons and microjets on jet noise. Chevron penetration is the underpinning factor for jet noise reduction and its optimum is found to be around one-seventh of the nozzle diameter. The number of chevrons has a considerable effect on jet noise and six is found to be an optimum number of chevrons. The injected mass flow rate of a system of microjets has a noticeable impact on jet noise and for 18 microjets its optimum is found to be around 0.0072 of the main jet mass flow rate. There is a good agreement between predicted and measured optimum values. This establishes that the model is indeed capable of assessing and optimising jet noise reduction concepts and could contribute towards the development of quieter nozzles for future aircraft.

---

\*Corresponding Author; AIAA Member; Email: nkd25@cam.ac.uk

†AIAA Fellow; Email: apd1@cam.ac.uk

## Nomenclature

$A$	Amplitude scale, $\text{m}^4/\text{s}^4$
$G_k$	Turbulent production, $\text{m}^2/\text{s}^3$
$k$	Turbulent kinetic energy, $\text{m}^2/\text{s}^2$
$l$	Length scale, m
$p$	Pressure, $\text{N}/\text{m}^2$
$R_{ijkl}$	Fourth-order space-time cross-correlations, $\text{m}^4/\text{s}^4$
$R_m$	Ratio of the injected mass flow rate per microjet to the main jet mass flow rate
$T_{ij}$	Source term, $\text{kg}/(\text{m}\text{-}\text{s}^2)$
$v$	Velocity, $\text{m}/\text{s}$
$\mathbf{x}$	Observer location, m
$\mathbf{y}$	Source location, m
$\rho$	Density, $\text{kg}/\text{m}^3$
$\mu$	Dynamic viscosity, $\text{kg}/(\text{m}\text{-}\text{s})$
$\xi$	Spatial separation, m
$\omega$	Streamwise vorticity, $\text{s}^{-1}$
$\Gamma$	Streamwise circulation, $\text{m}^2/\text{s}$
$\mu_t$	Turbulent viscosity, $\text{kg}/(\text{m}\text{-}\text{s})$
$\tau$	Time shift, s
$\eta$	Time scale, s
$\epsilon$	Turbulent dissipation rate, $\text{m}^2/\text{s}^3$
$\overline{(\ )}$	Time averaging
$\tilde{(\ )}$	Favre averaging

## I. Introduction

Jet noise is a dominant component of the overall aircraft noise, particularly at takeoff. With the introduction of advanced noise-reduction nozzles such as chevrons and microjets (figure 1), several experimental studies have been performed to achieve maximum jet noise reduction with minimum thrust loss. Bridges and Brown<sup>1</sup> found that chevron nozzles can significantly reduce jet noise, particularly at low-frequencies, but the benefits depend strongly on chevron angle and number of chevrons. Callendar *et al.*<sup>2</sup> have shown that nozzles with high number of chevrons have little impact on jet noise. This is due to the fact that the streamwise vortices generated by one chevron are cancelled by those of opposite sign generated by the next because the chevrons are so close to each other. Bridges and Brown<sup>1</sup> found

that there is an optimum number of chevrons beyond which the impact of chevrons on jet noise deteriorates. Although chevron nozzles increase high-frequency noise in the near-field of a jet, Callender *et al.*<sup>3</sup> argued that this does not necessarily lead to a comparable increase in the far-field of a jet because sound at high-frequency is attenuated by propagation through the atmosphere.

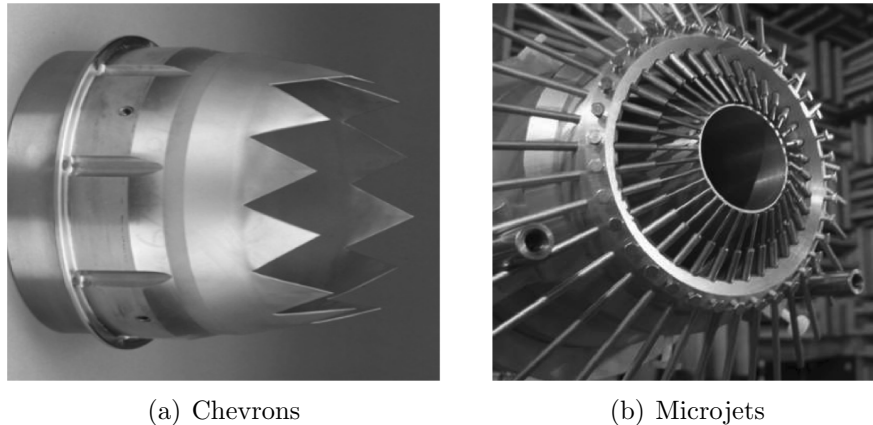


**Figure 1.** (a) Chevrons (Courtesy: NASA) (b) Microjets (Courtesy: Ecole Centrale de Lyon)

The main advantage of microjets, compared to chevrons, is their possibility of being turned off during cruise, which limits thrust loss to be only during takeoff. Arakeri *et al.*<sup>4</sup> showed that jet noise can be considerably reduced through steady injection of just 1% of the main jet mass flow. Castelain *et al.*<sup>5</sup> experimentally studied jet noise reduction as a function of the injected mass flow rate, the number and arrangement of microjets and the diameter of a microjet. The study on the microjet layout showed that the impact on jet noise is low when microjets were too close to each other and that certain configurations of microjet pairs could be favourable; this can be related to the flow structures induced by microjets. Zaman<sup>6</sup> observed a considerable jet noise reduction that improves with increasing microjet pressure. He found that smaller diameter ports with higher driving pressure, but involving less thrust and mass fraction, can produce better jet noise reduction. The results indicate that the overall sound pressure level correlates with the ratio of microjet to the main jet driving pressures normalised by the ratio of corresponding diameters. A physical understanding of the dependence of jet noise reduction on the ratio remains unclear. Henderson<sup>7</sup> reviewed the research on jet noise reduction through fluidic injection (both liquids and gases). Aqueous injection (water and steam for example) reduces noise by reducing the main jet temperature through evaporation and the main jet velocity through momentum transfer between the water droplets and the main jet, whereas gaseous injection (air for example) reduces the noise through the introduction of streamwise vortices and their effect on mixing. Although aqueous injection reduces jet noise up to 6 dB, it is not suitable for flight conditions as it

requires either large quantities of water or high injection pressures to achieve noise reduction. Although gaseous injection is suitable for flight conditions, it reduces jet noise only up to 2 dB.

Xia *et al.*<sup>8</sup> performed hybrid RANS–LES computations for chevron jets and they predicted jet noise using the Ffowcs Williams and Hawkings<sup>9</sup> acoustic analogy and a hybrid acoustic analogy<sup>10</sup> – the latter provided better jet noise predictions. Several researchers (Bodony and Lele<sup>11</sup> for example) have showed promising jet noise predictions using LES. Although LES provide accurate jet noise predictions, it is unlikely to use them for optimising nozzle designs as they are highly expensive and time consuming i.e. they take several months on a High Performance Computing system. On the other hand, RANS provide reasonably accurate jet noise predictions and they deliver quick results i.e. they take only a few days on a personal computer. This indicates that RANS could be an appropriate tool for the nozzle optimisation. Engel *et al.*<sup>12</sup> demonstrated that RANS–based methods are reliable to obtain jet noise predictions. RANS simulations were performed with a cubic k– $\epsilon$  turbulence model and jet noise was predicted by Lighthill Ray Tracing method. The flow and noise predictions were in a reasonably good agreement with measurements. However, there were major discrepancies at low frequencies where chevrons are known to have high impact on jet noise. Only a limited number of numerical works have been published on jet noise reduction through microjets (Enomoto *et al.*<sup>13</sup>; Laurendeau *et al.*<sup>14</sup>; Naja–Yazdi *et al.*<sup>15</sup>; Rife & Page<sup>16</sup> & Shur *et al.*<sup>17</sup>). The simulations show that LES can capture the effect of microjets on jet noise. However, there is not much research on the RANS–based jet noise modelling of chevrons and microjets, particularly in the subsonic flow regime.

In our previous study (Depuru Mohan *et al.*<sup>18</sup>), the noise of the chevron jet was predicted through applying Goldstein’s acoustic analogy in which the source statistics are described by  $R_{ijkl}(\mathbf{y}, \xi, \tau)$  the two–point two–time cross–correlations of the fluctuating Reynolds stresses,  $T'_{ij}$ , i.e.  $R_{ijkl}(\mathbf{y}, \xi, \tau) = \overline{T'_{ij}(\mathbf{y}, t)T'_{kl}(\mathbf{y} + \xi, t + \tau)}$ , where the overbar denotes the time average and the prime a perturbation from the mean.  $R_{ijkl}(\mathbf{y}, \xi, \tau)$  was modelled by a Gaussian function described by amplitude, length and time scales. It was found that RANS is able to capture the variation of these acoustic source scales with position within the jet and there is a proportionality between turbulence scales (taken from RANS) and acoustic source scales (taken from LES). The proportionality constants were determined by fitting RANS turbulence scales to on the acoustic source scales determined from LES and are found to be independent of source location and nozzle geometry. The acoustic sources were described by these derived RANS scales. However, the relative amplitudes of  $R_{ijkl}(\mathbf{y}, \mathbf{0}, 0)$  cross–correlations with respect to the  $R_{1111}(\mathbf{y}, \mathbf{0}, 0)$  cross–correlation were taken from LES. There was a very good agreement between the model’s jet noise predictions and measurements over a wide range of frequencies and observer angles. The effect of acoustic length scales,

proportionality constants and turbulence models on jet noise predictions were also studied. The accuracy of jet noise predictions can be significantly improved by taking into account of the anisotropy of acoustic length scales. There was an effect of 0.2 – 0.7 dB on jet noise predictions when the proportionality constants were varied by 10%. There was an effect of 0.5 dB on jet noise predictions depending on the turbulence model used.

The ultimate goal of chevrons or microjets is to provide maximum jet noise reduction with minimum thrust loss. To optimise a nozzle geometry during its design phase, a quick and accurate jet noise prediction model which does not depend on either LES nor on experiments is needed. The present study aims to address this need. The first objective of the present study is to develop a quick and accurate jet noise prediction model for chevron jets. To make the model independent of LES, the amplitude of the fourth-order space-time velocity cross-correlations is expressed in terms of mean flow parameters and turbulence statistics (such as streamwise circulation, axial velocity and turbulent kinetic energy) that can be obtained from RANS. A direct relationship between acoustic sources and streamwise vortices is investigated. Once such a model is established for chevron jets, the second objective of the present study is to perform a parametric study to find the important geometric parameters of chevrons for achieving jet noise reduction. The third objective of the present study is to apply the new model to microjets and perform a parametric study to identify the key factors (both flow and geometric) of microjets for achieving jet noise reduction.

## II. Flow Modelling

### A. RANS Modelling

The commercial software, ANSYS13.0 FLUENT, is used to perform RANS time-averaged flow calculations for chevron jets and microjets (main jet Mach number = 0.9 for both cases). As the jet flow is highly turbulent i.e. Reynolds number  $\approx 10^6$ , the standard  $k$ - $\epsilon$  turbulence model is chosen for the jet flow calculations. Only a sector of the  $360^\circ$  computational domain is considered as the jet mean flow is identical for each chevron or microjet. A mesh sensitivity study was performed and a 2.5 million-node mesh is found to provide quick and reasonably accurate predictions of the jet flowfield. Figure 2 shows the boundary conditions of RANS computational domain and figure 3 displays the mesh close to chevrons.

The FLUENT software obtains the jet flowfield by solving the time-average of the compressible Navier-Stokes equation given below,

$$\frac{\partial}{\partial t}(\rho v_i) + \frac{\partial}{\partial x_j}(\rho v_i v_j) = \frac{\partial \sigma_{ij}}{\partial x_j} \quad (1)$$

where

$$\sigma_{ij} = -p\delta_{ij} + \mu_t \left( \frac{\partial v_i}{\partial x_j} + \frac{\partial v_j}{\partial x_i} \right) \quad (2)$$

where  $p$  is pressure,  $v_i$  is velocity,  $\mu_t$  is eddy (or turbulent) viscosity and  $\rho$  is density. Although the present study is limited to unheated jets, the energy equation is solved:

$$\frac{\partial E}{\partial t} + \frac{\partial((E + p)v_i)}{\partial x_i} = S \quad (3)$$

where  $E = \rho e + 0.5\rho(u^2 + v^2 + w^2)$  is the total energy per unit volume, with  $e$  being the internal energy per unit mass of the fluid and  $S$  is the source term.

The standard  $k$ - $\epsilon$  turbulence model is based on the transport equations of turbulent kinetic energy,  $k$ , and its rate of dissipation,  $\epsilon$ . The transport equation for turbulent kinetic energy,  $k$ , is derived from the exact equation, whereas the transport equation for rate of dissipation of turbulent kinetic energy,  $\epsilon$ , is obtained using physical reasoning. The transport equations for turbulent kinetic energy,  $k$ , and turbulent dissipation,  $\epsilon$ , are:

$$\frac{\partial}{\partial t}(\rho k) + \frac{\partial}{\partial x_i}(\rho k v_i) = \frac{\partial}{\partial x_j} \left[ \left( \mu + \frac{\mu_t}{\sigma_k} \right) \frac{\partial k}{\partial x_j} \right] + G_k - \rho \epsilon \quad (4)$$

and

$$\frac{\partial}{\partial t}(\rho \epsilon) + \frac{\partial}{\partial x_i}(\rho \epsilon v_i) = \frac{\partial}{\partial x_j} \left[ \left( \mu + \frac{\mu_t}{\sigma_\epsilon} \right) \frac{\partial \epsilon}{\partial x_j} \right] + C_{1\epsilon} \frac{\epsilon}{k} G_k - C_{2\epsilon} \rho \frac{\epsilon^2}{k} \quad (5)$$

where  $v_i$  is mean velocity;  $G_k$  is turbulent production;  $\mu$  is dynamic viscosity;  $\mu_t$  is turbulent viscosity which is an added viscosity that appears due to the way turbulence is represented. It is defined as:  $\mu_t = \rho C_\mu k^2 / \epsilon$  where  $C_\mu = 0.09$ . In our flow calculations,  $C_{1\epsilon} = 1.44$ ;  $C_{2\epsilon} = 1.92$ ;  $\sigma_k = 1$  and  $\sigma_\epsilon = 1.3$  are taken as the turbulent Prandtl numbers for  $k$  and  $\epsilon$  respectively. As equations 1–5 are in unsteady form, they are iterated until a steady solution is obtained, thereby giving the mean flow. In our previous study (Depuru Mohan *et al.*<sup>18</sup>), the effect of different turbulence models on jet noise predictions was found to be less than 0.5 dB and the standard  $k$ - $\epsilon$  turbulence model provided accurate jet noise predictions. Hence, the standard  $k$ - $\epsilon$  turbulence model is chosen for the present study.

## B. LES Modelling

A hybrid RANS–ILES (Implicit LES) modelling (Xia *et al.*<sup>8</sup>) is used to simulate high-speed jet flows. The Favre–average Navier–Stokes equations are solved using a parallel finite volume in–house code. The Spalart–Allmaras RANS model (Spalart and Allmaras<sup>19</sup>) is used near the nozzle wall. The LES mesh has 69 blocks and nearly 20–million grid points. Figure 4 displays the LES mesh in various planes and figure 5 shows the boundary conditions of LES computational domain.

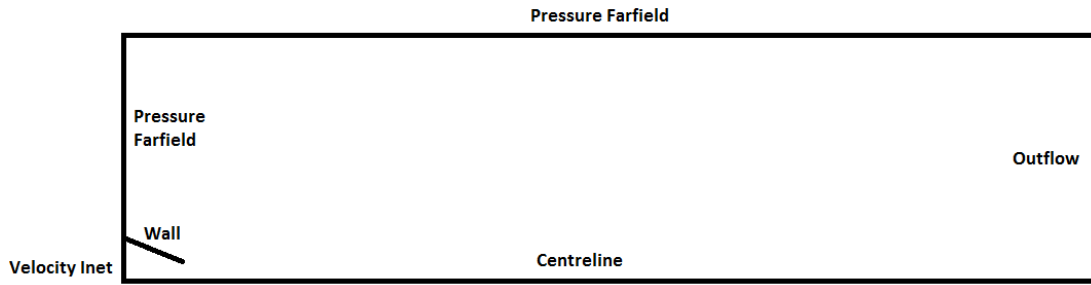


Figure 2. Boundary conditions of the RANS computational domain

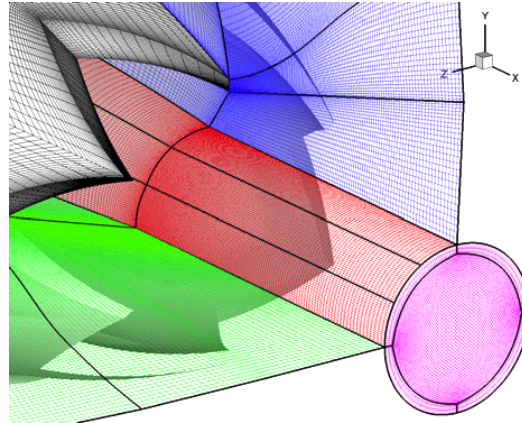


Figure 3. Mesh close to chevrons

The LES cases were run for approximately 300,000 time steps, with a physical time step of  $1.7 \times 10^{-7}$  seconds (maximum Courant–Friedrichs–Lewy (CFL) number  $\approx 0.3$ ). It took around 100,000 time steps to reach a fully–developed jet, another 100,000 time steps to capture the turbulence scales, and a further 100,000 time steps to obtain the acoustic scales. The extent of the three–dimensional LES computational domain is 72 jet diameters in the axial direction and 50 jet diameters in the radial direction for the entire  $360^\circ$  of the jet. The grid for a single chevron is generated first and replicated azimuthally. Multi–block type hexahedral grids were used to achieve high mesh accuracy. To avoid clustering of polar points or lines, a singularity treatment is done along the jet centreline. Xia and Tucker<sup>20</sup> have performed mesh sensitivity tests and discussed the effect of mesh size on noise predictions.

### III. Chevrons

#### A. Nozzle Geometry

Figure 6 shows the terminology of a chevron nozzle geometry. In the first instance of this study, SMC006 chevron nozzle is analysed, which has a chevron count of six, chevron length of 22.6 mm and chevron angle of  $18.2^\circ$  and an effective diameter of 47.7 mm. For comparison

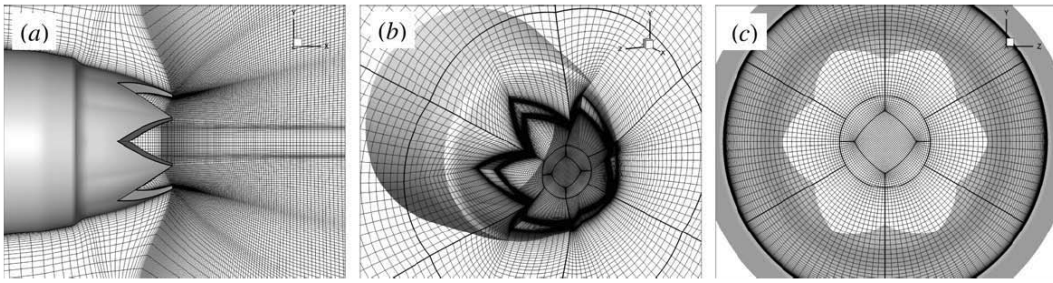


Figure 4. LES mesh: (a) XY plane; (b) X slice through the chevron edge; (c) YZ (jet inlet) plane. (Courtesy: Xia and Tucker<sup>21</sup>)

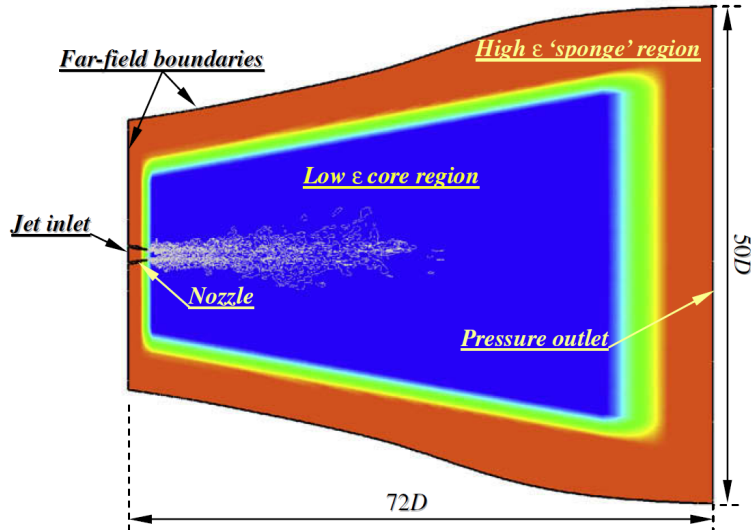


Figure 5. Boundary conditions of the LES computational domain (Courtesy: Xia and Tucker<sup>21</sup>)

purposes, SMC000 round nozzle is analysed, which has an effective diameter of 50.8 mm. The effective diameter was determined experimentally by assuming the discharge coefficient to be the same for both chevron and round nozzles and the measured mass flow was used as a surrogate area measurement.

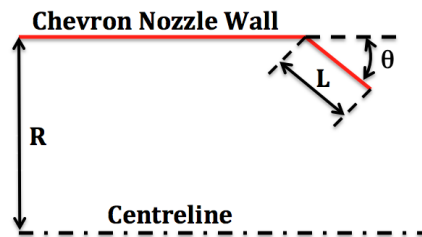


Figure 6. Chevron nozzle geometry terminology:  $L$  is the chevron length;  $\theta$  is the chevron angle and  $R$  is the nozzle radius

## B. Flow Results

Figure 7 shows that the mean centreline velocity decays dramatically beyond four jet diameters from the nozzle exit. Figure 8 shows that the turbulence intensity attains its maximum value just downstream of the break-down of the jet potential core. There is a good agreement between RANS predictions and measurements (Bridges and Brown<sup>1</sup>). Figure 9 shows the contours of streamwise vorticity generated by the chevron jet. When the jet flow is obstructed by the chevron tips, it tries to escape around the chevron slants and through the chevron roots. This generates two counter-rotating streamwise vortices of equal strength at each chevron tip. The figure also shows that streamwise vortices generated by the chevron jet decay by four jet diameters from the nozzle exit. These streamwise vortices enhance mixing between the jet and ambient air. This vortex-enhanced mixing could lead to jet noise reduction.

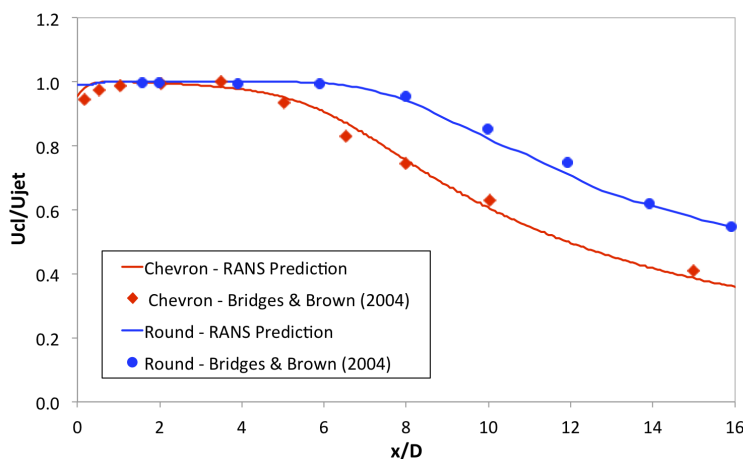


Figure 7. The centreline velocity decay of the jet

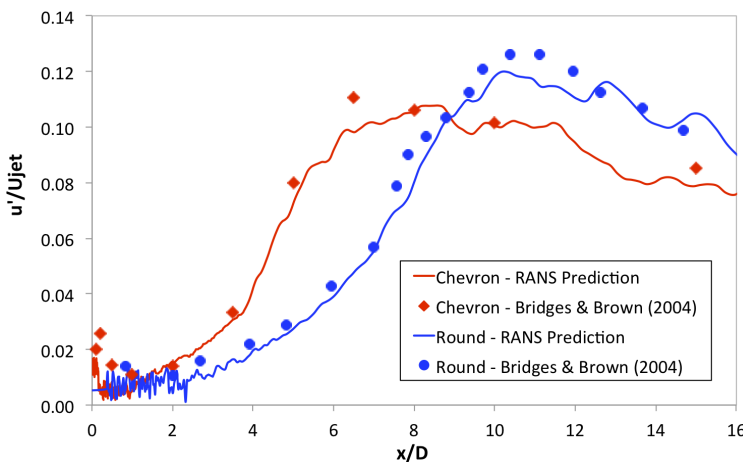
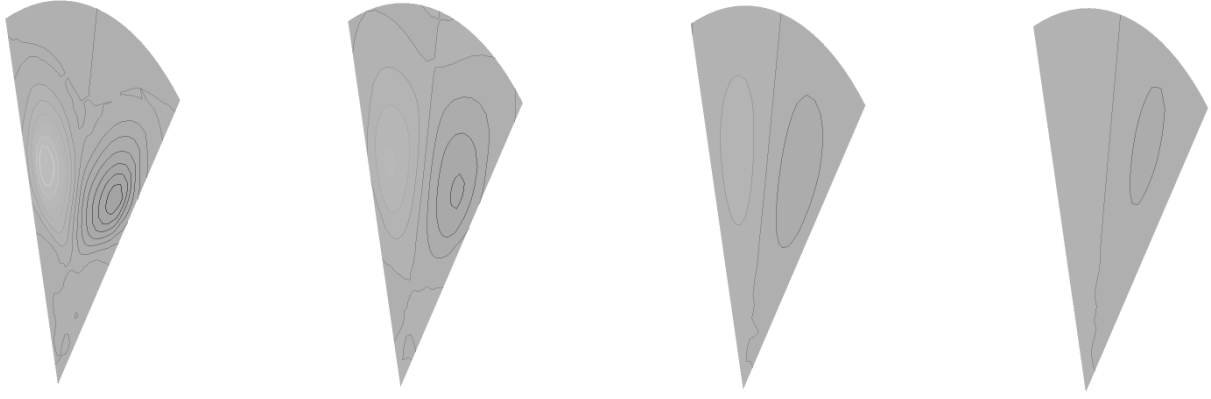
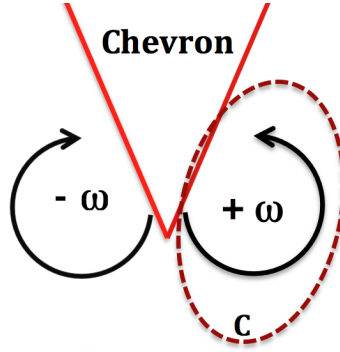


Figure 8. Turbulence intensity along the jet centreline



**Figure 9.** Contours of streamwise vortices generated by the chevron jet (SMC006) at  $x/D = 1, 2, 3$  and  $4$  respectively (from left to right);  $-1.2$  (white)  $< \omega_x D/U_{jet} < +1.2$  (black); streamwise vortices are usually generated around the chevron nozzle lip ( $r = 0.5D$ )

The streamwise circulation is calculated by integrating streamwise vorticity ( $\omega$ ) over a surface area ( $A$ ) enclosed by the contour ( $C$ ) that is taken around one of the two streamwise vortices generated by a chevron as shown in figure 10. Figure 11 shows that RANS captures the decay of streamwise circulation along axial distance very well although RANS predictions are not as accurate as LES predictions.



**Figure 10.** The contour 'C' (the brown dotted line) is taken just around a single vortex for the calculation of streamwise circulation. The streamwise circulation ( $\Gamma$ ) is calculated by integrating the streamwise vorticity ( $\omega$ ) over an area enclosed by the contour 'C'. The shape and size of the contour changes with the axial location.

### C. Description of Jet Noise Sources

The sources of jet noise are described by the fourth-order space-time velocity cross-correlations as below:

$$R_{ijkl}(\mathbf{y}, \xi, \tau) = \overline{T'_{ij}(\mathbf{y}, t) T'_{kl}(\mathbf{y} + \xi, t + \tau)} \quad (6)$$

where

$$T'_{ij} = -(\rho v_i'' v_j'' - \bar{\rho} \widetilde{v_i'' v_j''}) \quad (7)$$

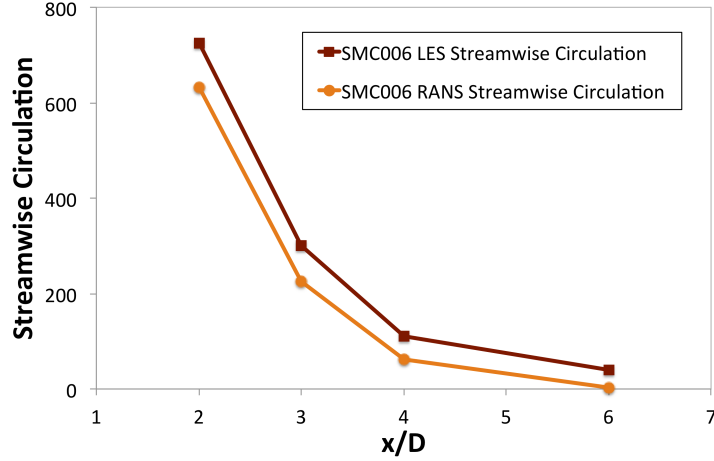


**Figure 11. Streamwise circulation – comparison of LES and RANS predictions**

where  $\mathbf{y}$  is the source location;  $\xi$  is spatial separation;  $\tau$  is the time shift;  $t$  is time;  $\rho$  is density;  $v''$  is fluctuating velocity and  $\widetilde{(\ )}$  represents Favre averaging. Although  $R_{1111}$  is the dominant cross-correlation, the other considerable cross-correlations are  $R_{2222}$ ,  $R_{3333}$ ,  $R_{1212}$ ,  $R_{1313}$ ,  $R_{2323}$  and the cross-correlations equal to them by symmetry. All these major cross-correlations have the shape of the following Gaussian form.

$$R_{1111}(\mathbf{y}, \xi, \tau) = A \exp \left[ -\frac{\xi_1}{\bar{v}\eta} - \ln 2 \left( \frac{(\xi_1 - \bar{v}\tau)^2}{l_1^2} + \frac{\xi_2^2}{l_2^2} + \frac{\xi_3^2}{l_3^2} \right) \right] \quad (8)$$

where  $A$  is the amplitude scale;  $\eta$  is time scale;  $l_1$ ,  $l_2$  and  $l_3$  are axial, radial and azimuthal length scales respectively;  $\xi_1$ ,  $\xi_2$  and  $\xi_3$  are spatial separations in the axial, radial and azimuthal directions respectively;  $\bar{v}$  is the mean axial velocity at location  $\mathbf{y}$ . The acoustic source scales  $A$ ,  $\eta$ ,  $l_1$ ,  $l_2$  and  $l_3$  are determined by curve fitting the Gaussian form (equation 8) onto the cross-correlations (equation 6) obtained from LES. The acoustic source scales are also calculated based on RANS standard  $k$ - $\epsilon$  turbulence model: amplitude scale,  $A = k^2$ ; time scale,  $\eta = k/\epsilon$  and length scale,  $l = k^{3/2}/\epsilon$  where  $k$  is turbulent kinetic energy and  $\epsilon$  is the rate of dissipation of turbulent kinetic energy.

In our previous study (Depuru Mohan *et al.*<sup>18</sup>), we found that RANS can capture the variation of amplitude, length and time scales with source location. We found that there is a proportionality between turbulence (RANS) and acoustic (LES) scales. The constants of proportionality for amplitude, time and length (axial, radial and azimuthal) scales were found to be 1.0, 0.14, 0.26, 0.08 and 0.08 respectively. These constants of proportionality were found to be independent of both nozzle geometry and source location. Therefore, these constants of proportionality are used in the present study.

In our previous study (Depuru Mohan *et al.*<sup>18</sup>), the relative magnitudes of  $R_{ijkl}(\mathbf{y}, \mathbf{0}$ ,

0) cross-correlations with respect to the  $R_{1111}(\mathbf{y}, \mathbf{0}, 0)$  cross-correlation were taken from LES. In the present study, a novel equation is proposed to express the amplitude of the fourth-order space-time velocity cross-correlations in terms of mean flow parameters and turbulence statistics that can be obtained from RANS. The cross-correlations at zero spatial separation ( $\xi = \mathbf{0}$ ) and zero time shift ( $\tau = 0$ ) are given by,

$$R_{ijkl}(\mathbf{y}, \mathbf{0}, 0) = \overline{T'_{ij}(\mathbf{y}, t) T'_{kl}(\mathbf{y}, t)} \quad (9)$$

The relationship between the fourth-order space-time cross-correlations and the jet flow parameters that can be obtained from RANS is investigated. SMC006 chevron and SMC000 round jets are analysed for this purpose. Equation 10 shows that the cross-correlations are proportional to the square of turbulent kinetic energy.

$$R_{ijkl}(\mathbf{y}) = \alpha_{ijkl} * \bar{\rho}^2 * k(\mathbf{y})^2 \quad (10)$$

LES results for a round jet show that  $\alpha_{ijkl} = 1.0$  for  $R_{1111}$ ; 0.4 for  $R_{2222}$  and  $R_{3333}$ ; 0.34 for  $R_{1212}$  and  $R_{1313}$ ; 0.2 for  $R_{2323}$ . These constants hold good throughout the round jet as shown in Figure 12. In contrast, for a chevron jet while the ratio of the amplitude of  $R_{1111}$  cross-correlation to the square of turbulent kinetic energy is constant, the ratio for  $R_{2222}$  and  $R_{3333}$  cross-correlations decreases up to four jet diameters downstream and then it becomes roughly constant and equal to the round jet level.

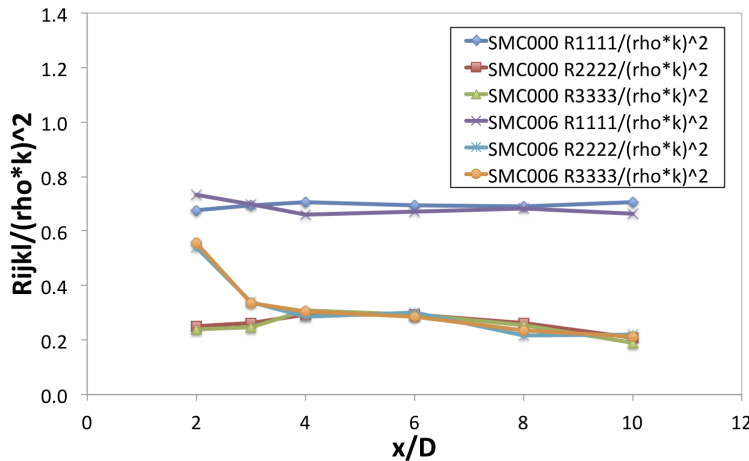


Figure 12. The variation of  $R_{ijkl}/(\bar{\rho} * k)^2$  with axial distance

The streamwise vortices generated by a chevron nozzle decay by four jet diameters from the nozzle exit. This prompted us to ask if there could be a proportionality between streamwise vorticity and the amplitude of  $R_{2222}$  and  $R_{3333}$  cross-correlations. Figure 13 shows that the variation of the cross-correlations,  $R_{ijkl}$ , tracks the variation of streamwise circulation ( $\Gamma$ ).

$$R_{ijkl}(\mathbf{y}) \propto \Gamma(\mathbf{y}) \quad (11)$$

where  $\Gamma$  is defined as,

$$\Gamma = \int_A \omega dA \quad (12)$$

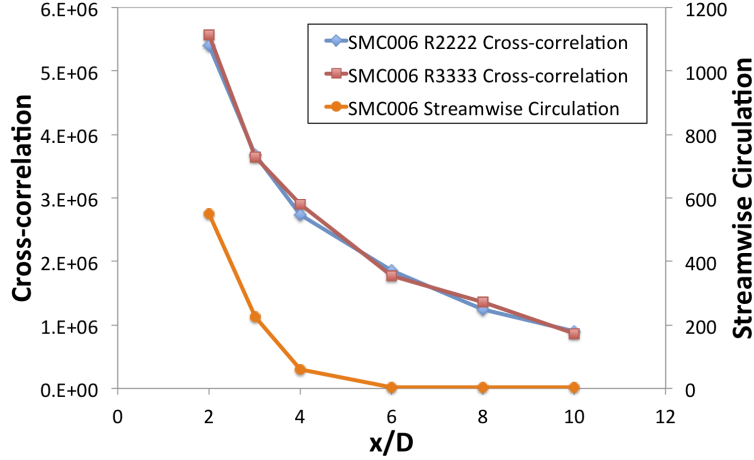


**Figure 13.** The proportionality between  $R_{2222}$  and  $R_{3333}$  cross-correlations and streamwise circulation

This also makes physical sense, since streamwise circulation is expected to increase the in-plane velocity fluctuations. This enabled us to propose a novel equation for the fourth-order space-time velocity cross-correlations. The equation 13 is the sum of two terms; the first one is proportional to the square of turbulent kinetic energy and the second one is a combination of streamwise circulation, turbulent kinetic energy and local axial velocity. This equation involves two constants:  $\beta_{ijkl}$ , is found by curve-fitting LES results for the SMC006 chevron jet and  $\alpha_{ijkl}$  is based on the analysis of a round jet where it is the ratio of the amplitude of a cross-correlation to the square of turbulent kinetic energy. Both  $\alpha_{ijkl}$  and  $\beta_{ijkl}$  are to be the same constants throughout the entire jet.

$$R_{ijkl}(\mathbf{y}) = \alpha_{ijkl} * \bar{p}^2 * k(\mathbf{y})^2 + \beta_{ijkl} * \bar{p}^2 * k(\mathbf{y}) * \bar{u}(\mathbf{y})^2 * \Gamma(\mathbf{y}) / (U_{jet} * D_{jet}) \quad (13)$$

where as already noted  $\alpha_{ijkl} = 0.7$  for  $R_{1111}$ ;  $0.27$  for  $R_{2222}$  and  $R_{3333}$ ;  $0.23$  for  $R_{1212}$  and  $R_{1313}$ ;  $0.14$  for  $R_{2323}$ ;  $\beta_{ijkl}$  was found to be zero for  $R_{1111}$  and  $0.07$  for the other cross-correlations;  $\mathbf{y}$  is the source location;  $k$  is turbulent kinetic energy;  $\bar{u}$  is mean axial velocity;  $\Gamma$  is streamwise circulation,  $U_{jet}$  is the jet velocity at the nozzle exit and  $D_{jet}$  is the jet diameter.

The  $R_{1111}$  cross-correlation depends only on turbulent kinetic energy, whereas  $R_{2222}$ ,  $R_{3333}$ ,  $R_{1212}$ ,  $R_{1313}$ ,  $R_{2323}$  and other cross-correlations equal to them by symmetry are also

affected by streamwise vorticity. For a round jet, the second term on the right-hand side of equation 13 is effectly zero as it has negligible streamwise vorticity. Therefore, the equation 13 applies to both chevron and round jets. Figure 14 shows that using equation 13 gives a good agreement between the amplitude of the cross-correlations based on RANS and LES flowfields. Figure 15 confirms that equation 13 for the amplitude of the cross-correlation is valid for other radial locations. The equation 13 rather implies that there is a direct link between the mean jet flow and its turbulent kinetic energy and the acoustic sources. This establishes that RANS can be used to describe jet noise sources accurately.

#### D. Calculation of Far-field Jet Noise

The sound propagation from the noise sources to the jet far-field is determined through the calculation of the Green's function – the solution of the adjoint Linearised Euler Equations. With a numerical solution, the effects of scattering by a nozzle and the axial development of a jet mean flow (Karabasov *et al.*<sup>10</sup>) can be included. Instead, for simplicity, a locally parallel jet flow approximation (Tam and Aurialt<sup>22</sup>) is made. Then the Green's function can be quickly calculated analytically. The sound power spectral density (PSD) is the end result of sound propagation calculations, which is expressed as,

$$\hat{P}(\mathbf{x}, \omega) = \int_{V_\infty(\mathbf{y})} \int_{\xi} \hat{R}_{ijkl}(\mathbf{y}, \xi, \omega) \hat{I}_{ij}(\mathbf{y}, \omega|\mathbf{x}) \hat{I}_{kl}(\mathbf{y} + \xi, -\omega|\mathbf{x}) d^3\xi d^3\mathbf{y} \quad (14)$$

where  $\mathbf{x}$  is the observer location;  $\mathbf{y}$  is the source location;  $\hat{I}_{ij}$  and  $\hat{I}_{kl}$  are the Fourier transform of second-rank wave propagation tensors and  $\hat{R}_{ijkl}$  is the Fourier transform of fourth-order space-time cross-correlations, which is given by

$$\hat{R}_{ijkl}(\mathbf{y}, \xi, \omega) = \int R_{ijkl}(\mathbf{y}, \xi, \tau) e^{-i\omega\tau} d\tau = \int \overline{T'_{ij}(\mathbf{y}, t) T'_{kl}(\mathbf{y} + \xi, t + \tau)} e^{-i\omega\tau} d\tau \quad (15)$$

To validate the model's jet noise predictions, round and chevron nozzles are chosen from Bridges and Brown<sup>1</sup> experimental study. All these nozzles are thrust-equivalent with the following flow conditions at their exit: Reynolds number  $\approx 1.03 \times 10^6$ ; Mach number = 0.9 and temperature ratio = 0.84. The geometric details of the chosen nozzles are provided in table 1 and photographs of the chosen nozzles are shown in figure 16.

Nozzle ID	Chevron Count	Chevron Length (mm)	Chevron Angle (deg)	Effective Diameter (mm)
SMC000	—	—	—	50.8
SMC006	6	22.6	18.2	47.7

**Table 1. Geometric details of the chosen nozzles (Bridges and Brown<sup>1</sup>)**

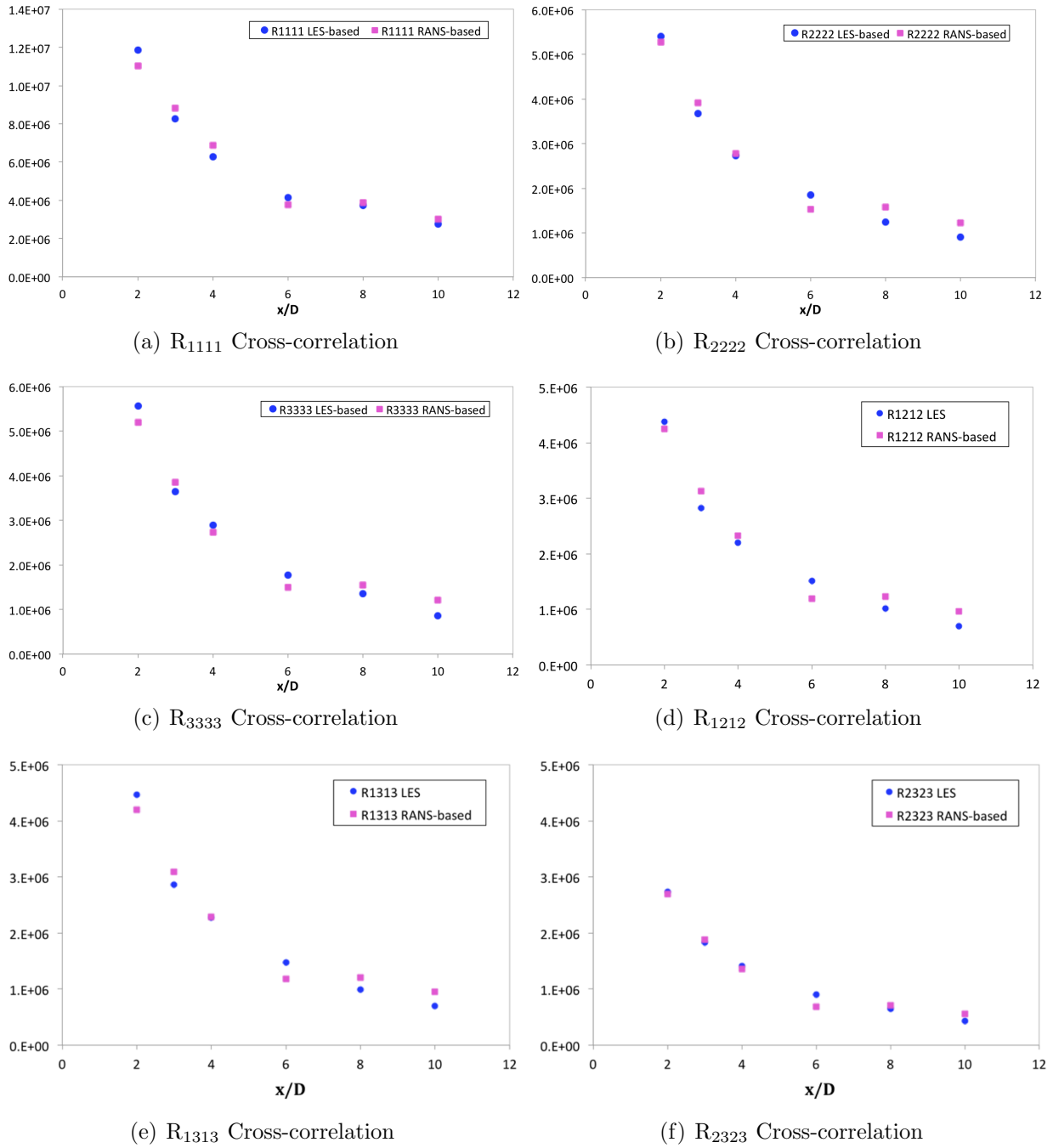


Figure 14. Comparison of LES-based and RANS-based cross-correlations at  $r/D = 0.5$

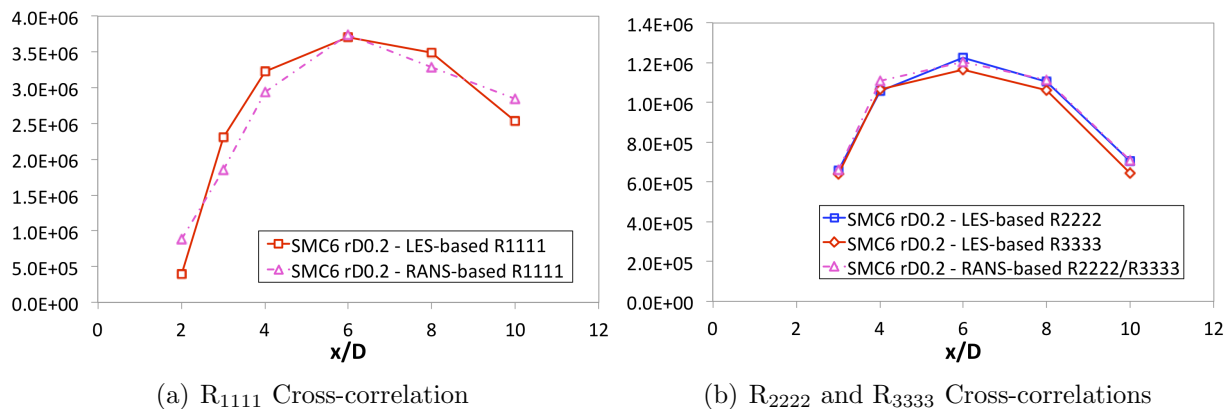


Figure 15. Comparison of LES-based and RANS-based cross-correlations at  $r/D = 0.2$

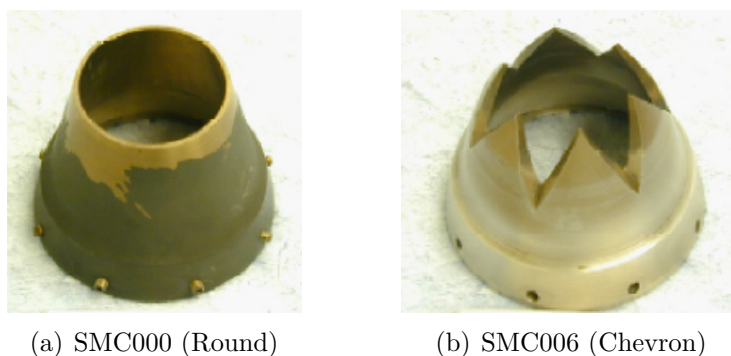


Figure 16. Photographs of the chosen nozzles (Bridges and Brown<sup>1</sup>)

Figure 17 shows that there is an excellent agreement between the model's jet noise predictions and measurements (Bridges and Brown<sup>1</sup>) at a distance of 40 jet diameters from the nozzle exit. For both chevron and round jets, they match very well for a wide range of frequencies and observer angles. The spectral shape has a sharp peak and faster roll-off at  $30^\circ$ , whereas it is flat and broad at  $90^\circ$  to the jet axis. The peak Strouhal number is approximately 0.2 at these two observer angles. The model captures both the spectral shape and peak Strouhal number. However, there are minor discrepancies at low frequencies. At  $30^\circ$  to the jet axis, the chevron nozzle has significantly reduced low-frequency noise compared to that of the round nozzle, i.e. for  $St \leq 0.2$ , the far-field jet noise is reduced by 5–6 dB (figure 17). This shows the strong impact of the chevron nozzle on jet noise reduction, particularly at low frequencies. However, there is no benefit at high frequencies. At  $90^\circ$  to the jet axis, the chevron nozzle has reduced low-frequency noise compared to that of the round nozzle, i.e. for  $St \leq 0.2$ , the far-field jet noise is reduced by 2–3 dB (figure 17). Hence the chevron nozzle has reduced low-frequency noise for a wide range of observer angles. However, the chevron nozzle has slightly increased high-frequency noise compared to that of the round nozzle. In the high frequency range (i.e.  $2 \leq St \leq 10$ ), there were discrepancies

between the model’s predictions and the experimental data. This is possibly due to the fact that the wave propagation model is too simple to capture high–frequency noise. In addition, a sensitivity study was performed to estimate the effect of  $\alpha$ ,  $\beta$  and the proportionality constants on the far-field noise predictions. The change in noise predictions was found to be around 0.5 dB when these constants were varied by 20%. This shows that the model is not so sensitive to these constants.

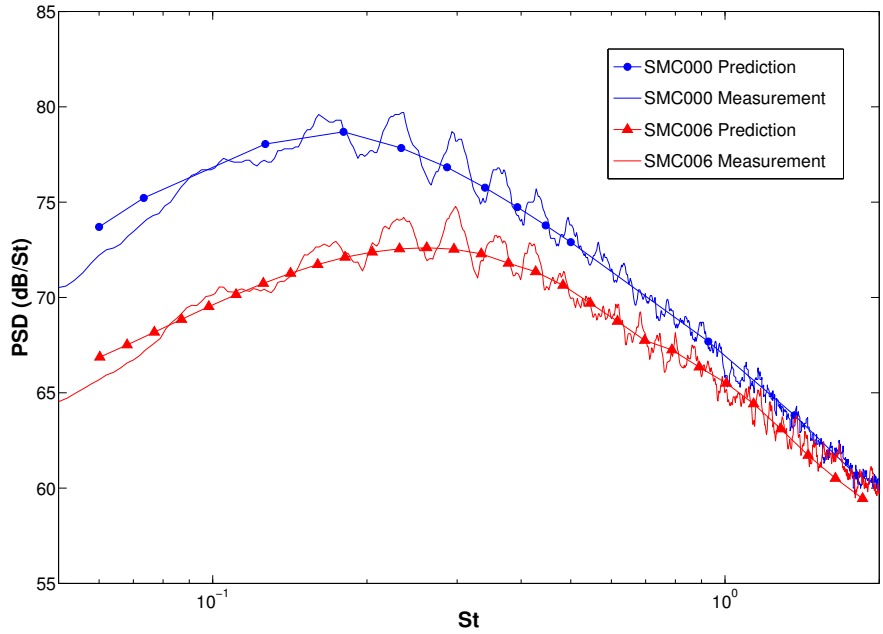
## E. Parametric Study

To investigate the impact of chevron geometric parameters on jet noise and thrust loss, a parametric study is performed using ANSYS13.0 Workbench. The geometric changes to the chevron nozzle are made in DesignModeler and then the computational mesh is generated. With this updated geometry and mesh, the flow calculations are performed in FLUENT. This RANS flowfield is used to calculate jet noise and thrust loss. The same procedure is repeated for each case of the parametric study. In the present study, chevron count is varied from 4 to 10; chevron angle is varied from 0 to  $30^0$  and chevron length is varied from 0 to 30 mm.

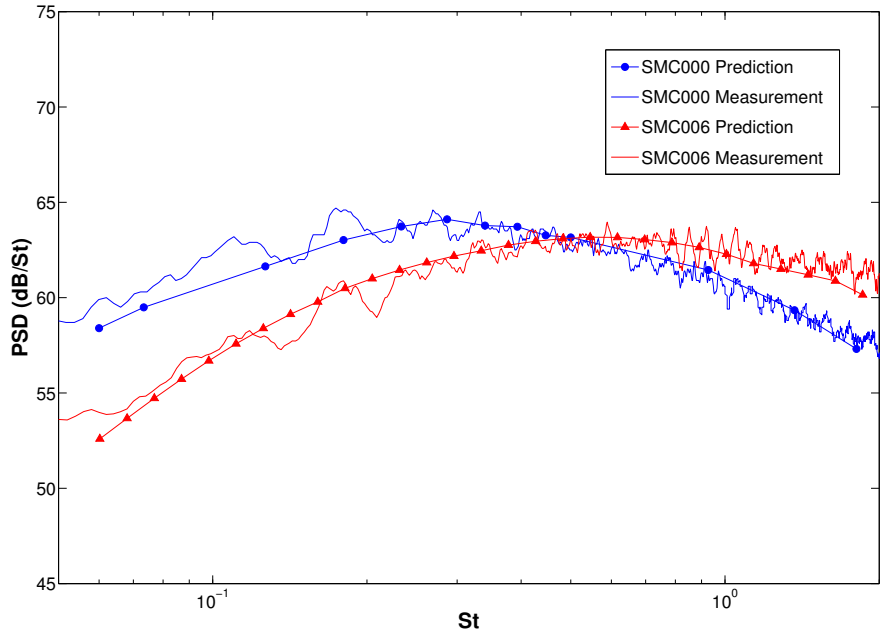
For the parametric study, the nozzle geometry is simplified by connecting chevron roots and tips by a straight line rather than a slightly curved line which is used in the original geometry (figure 16). It is expected that this small change should not affect the jet noise predictions. To confirm this, jet noise predictions based on the simplified nozzle geometry are compared with measurements (Bridges and Brown<sup>1</sup>) based on the original nozzle geometry. Figure 18 shows that there is a good agreement between the two for SMC005 and SMC006 chevron nozzles. This confirms that the simplified nozzle geometry does not affect jet noise predictions.

A family of chevron nozzles are investigated to understand the effect of chevron count, angle and length on jet noise and thrust loss. Figure 19 shows that there is a significant increase in jet noise reduction with an increase of chevron angle. However, nozzles with aggressive chevron angles lead to major thrust loss. There is a significant jet noise reduction from a round nozzle for a  $5^0$  chevron angle and then the change becomes less dramatic with further increases in chevron angle. Figure 20 shows that there is a considerable jet noise reduction up to a chevron count of six and then the effect of chevrons deteriorate with further increase in chevron count. Figure 21 shows that jet noise reduction increases with chevron length, but nozzles with large chevron lengths lead to major thrust loss.

Chevron penetration is defined as the radial distance by which a chevron penetrates into the jet flow. By definition, chevron penetration is a product of chevron length and the sine of chevron angle. Figure 22 shows that jet noise reduction is comparable for chevron nozzles that have the same penetration and the same number of chevrons. Chevron penetration is



(a)  $30^\circ$  to the jet axis



(b)  $90^\circ$  to the jet axis

**Figure 17. Comparison of the model’s far-field jet noise predictions with measurements (Bridges and Brown<sup>1</sup>)**

found to be the underpinning factor for jet noise reduction. For small chevron penetrations, the jet noise reduction per unit thrust loss is constant as the chevron penetration is increased,

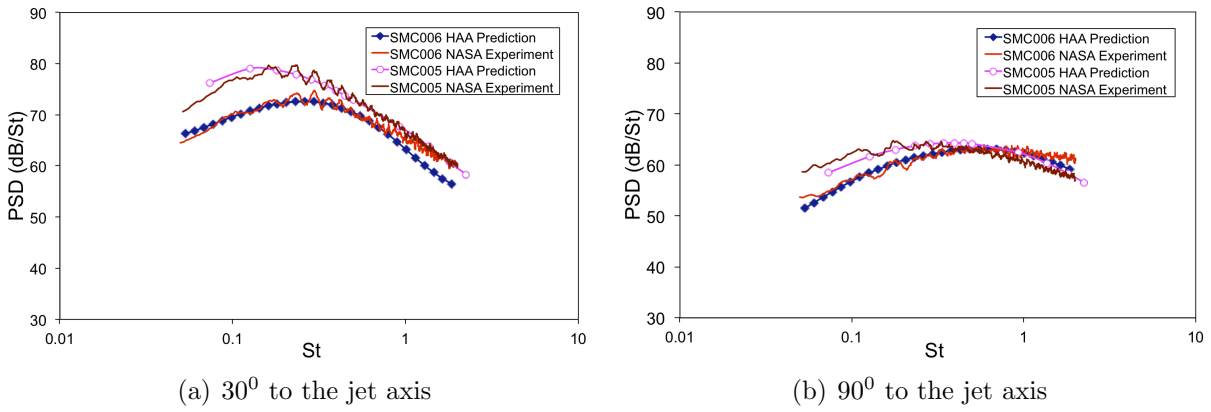


Figure 18. Jet noise predictions based on the simplified chevron nozzle geometry

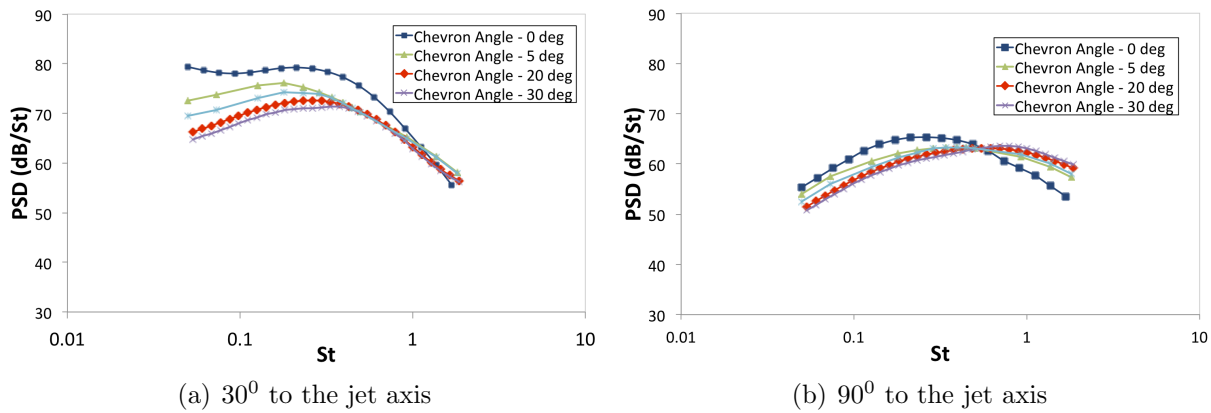


Figure 19. Effect of chevron angle on jet noise (count = 6 and length = 20 mm)

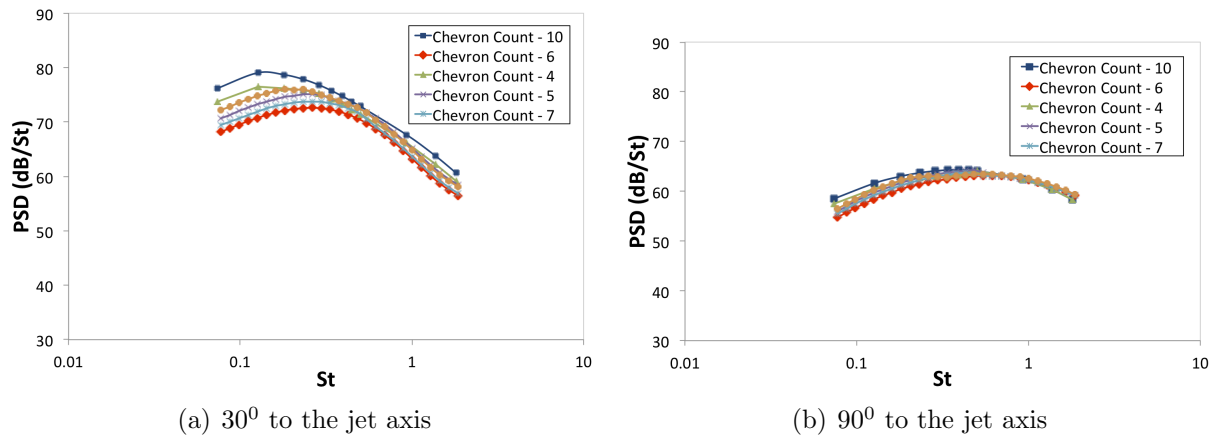


Figure 20. Effect of chevron count on jet noise (angle = 30 degrees and length = 20 mm)

indicating that the jet noise reduction (in dB) varies linearly with the thrust loss (in %). For chevron penetrations larger than one-seventh of the nozzle diameter, the thrust loss

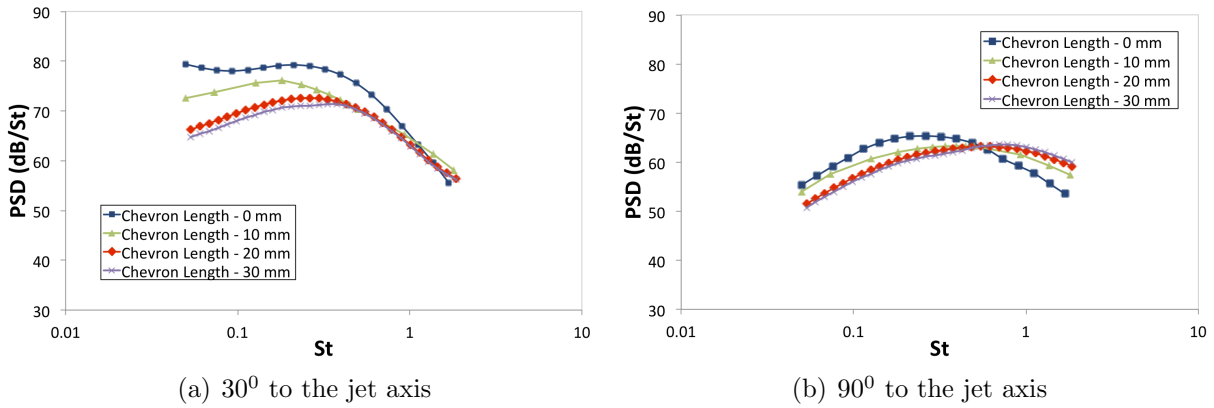


Figure 21. Effect of chevron length on jet noise (angle =  $30^\circ$  and count = 6)

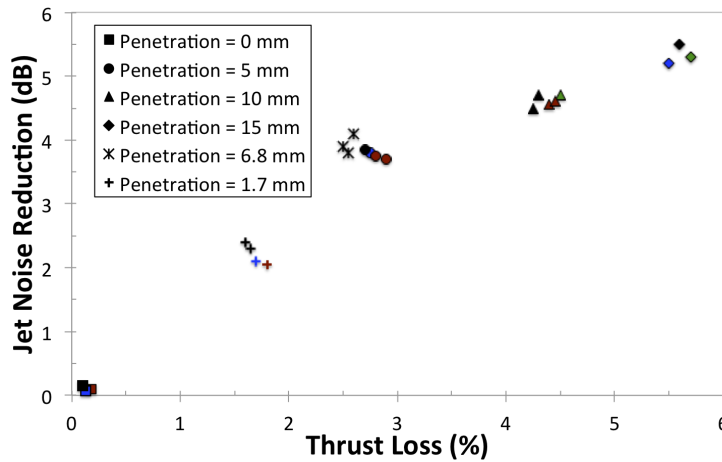


Figure 22. Effect of chevron penetration on jet noise reduction and thrust loss; symbols represent chevron penetration and colours represent chevron count – blue 4; brown 5; black 6; green 7 respectively

increases more rapidly with chevron penetration than the jet noise reduction. The figure also shows that chevron count has a considerable effect on jet noise and six is found to be an optimum number of chevrons.

## IV. Microjets

As the validation in figure 17 shows that the model works very well for chevron jets. It is now applied to a main jet modified by microjets, validated by comparison with experiment and then a parametric study is performed to quantify the effect of microjets on jet noise.

Castelain *et al.*<sup>5</sup> have experimentally showed that 18 is an optimum number of microjets for maximum jet noise reduction. In the experimental investigations, the diameter of the main jet and microjets are 0.022 m and  $400 \mu\text{m}$  (Arakeri *et al.*<sup>4</sup>); 50mm and 1mm respectively

(Castelain *et al.*<sup>5</sup>). In both cases, the diameter ratio (microjet to the main jet) is around 0.02 and the angle,  $\alpha$ , between the axes of the main jet and microjets is  $45^\circ$  (figure 23). In the present study, the effect of 18 microjets on the main jet (both at Mach 0.9), with a diameter ratio of around 0.02, is investigated.

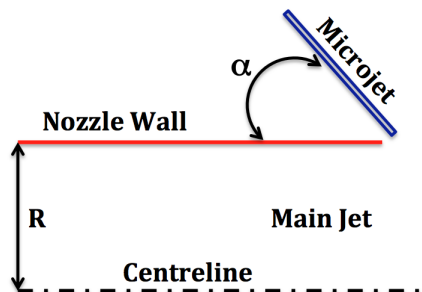


**Figure 23.** Microjets terminology:  $\alpha$  is the angle between the axes of the main jet and microjets (18 in number around the circumference of the main jet)

## A. Flow Results

Microjets affect the main jet flow up to two jet diameters from the nozzle exit. Figure 24(a) shows that the centreline velocity decay is captured reasonably well by RANS. Figure 24(b) shows that the centreline turbulence intensity attains its maximum value after the breakdown of the potential core. Figure 25 shows contour plots of the streamwise vorticity generated by microjets. Streamwise vortices generated by microjets are much weaker than those generated by chevron jets and they decay within two jet diameters (compared to four jet diameters in the case of chevron jets) from the nozzle exit. These factors lead to jet noise reduction through vortex-enhanced mixing. Overall, RANS captures the effect of microjets on the main jet flow reasonably well.

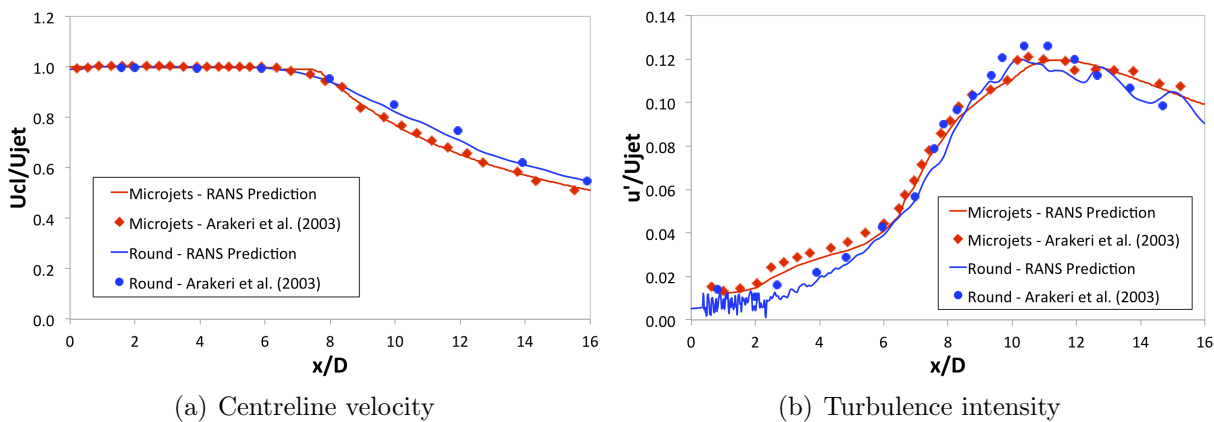


**Figure 24.** The main jet flow parameters in the presence of microjets

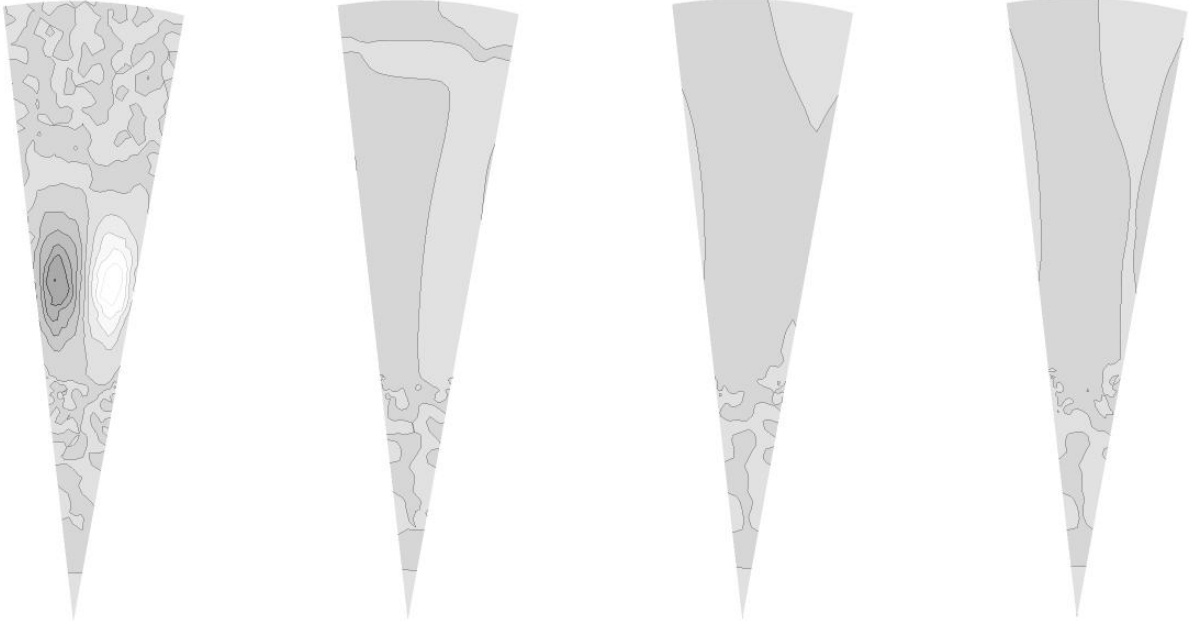


**Figure 25.** Contours of streamwise vortices generated by microjets at  $x/D = 1, 2, 3$  and  $4$  respectively (from left to right);  $-1.2$  (white)  $< \omega_x D / U_{jet} < +1.2$  (black); streamwise vortices are usually generated around the main nozzle lip ( $r = 0.5D$ )

## B. Azimuthal Variation of Source Scales

The sources of jet noise are described by the novel source description as explained in section §III.C. The acoustic source scales are calculated based on RANS standard  $k$ - $\epsilon$  turbulence model: amplitude scale,  $A = k^2$ ; time scale,  $\tau = k/\epsilon$  and length scale,  $l = k^{3/2}/\epsilon$  where  $k$  is turbulent kinetic energy and  $\epsilon$  is the rate of dissipation of turbulent kinetic energy. Figure 26 shows that the acoustic source scales become independent of azimuthal angle by two jet diameters from the nozzle exit. This is the region where microjets have a noticeable impact on both flow and acoustics.

## C. Calculation of Far-field Jet Noise

With the novel acoustic source description as expressed in equation 13 and same proportionality constants as that of chevron and round jets, figure 27 shows that there is an excellent agreement between the model's noise predictions and measurements. Microjets affect the shear layer of the main jet and reduce jet noise by 2 dB. More jet noise reduction is observed at  $30^\circ$  than at  $90^\circ$  to the jet axis. There is almost a 3 dB jet noise reduction at the peak frequency at  $30^\circ$  to the jet axis. However, there is an increase in the high-frequency noise. The model captures both the spectral shape and peak frequency very well. The model also predicts the cross-over of the high-frequency noise increase and low-frequency noise decrease.

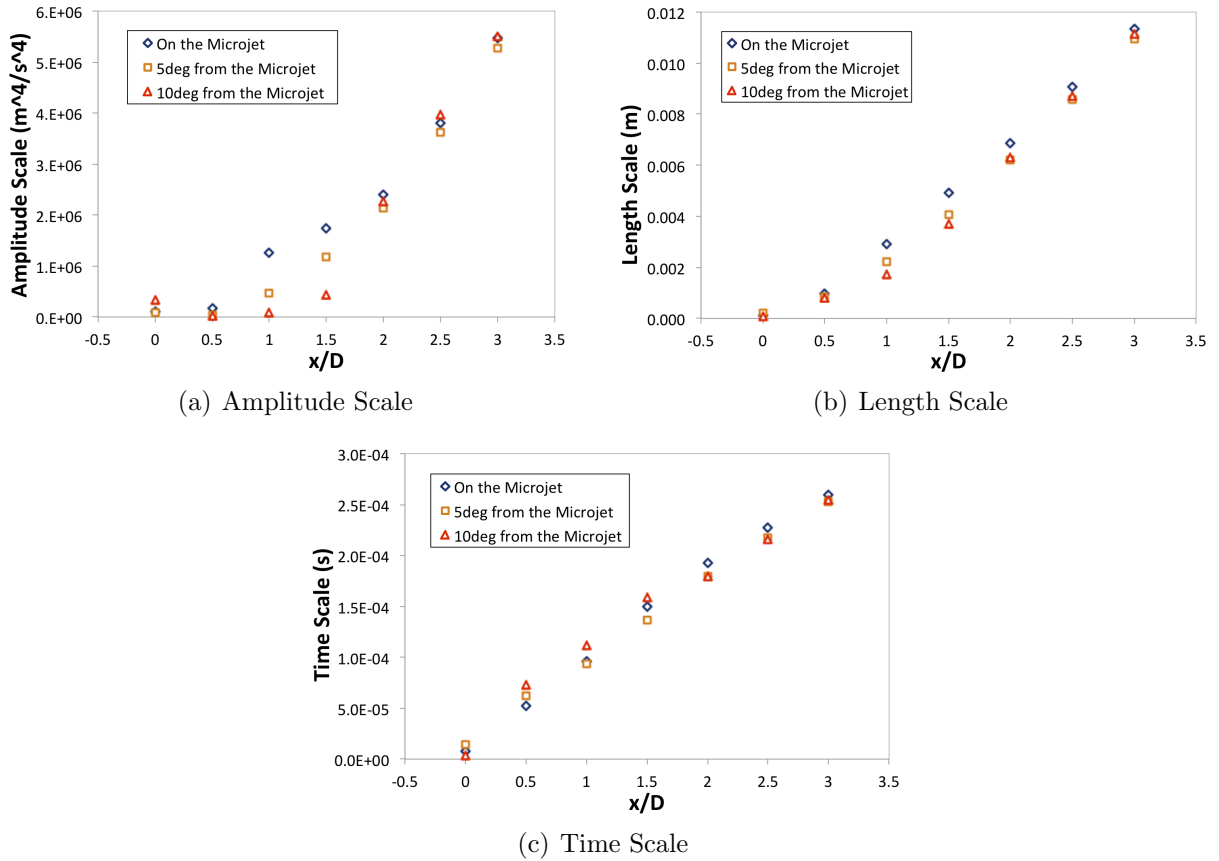


Figure 26. Azimuthal variation of the acoustic source scales

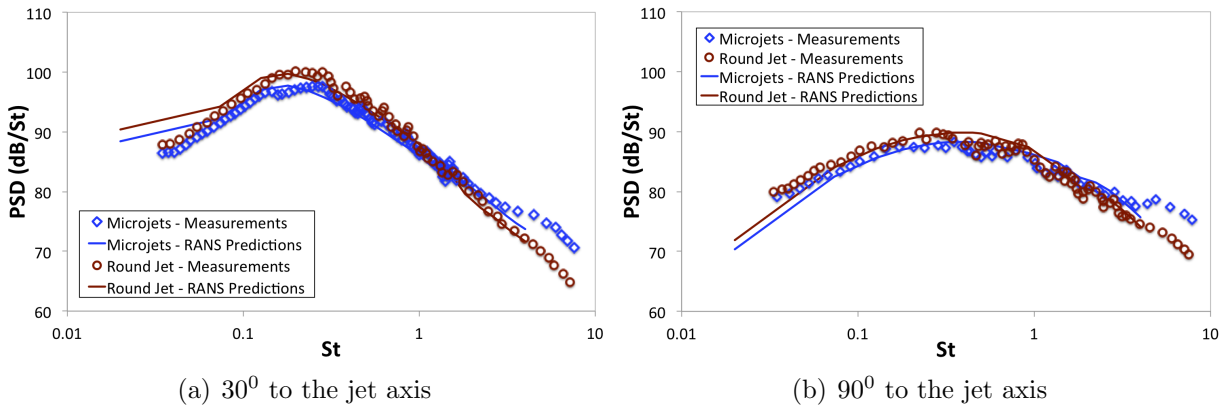


Figure 27. Comparison of the model's jet noise predictions with measurements

#### D. Parametric Study

To investigate the impact of microjets on jet noise, a parametric study is performed using ANSYS13.0 Workbench. The nozzle geometry changes are made in DesignModeler and then the computational mesh is generated. With this updated geometry and mesh, the boundary

conditions are applied and the flow calculations are performed in FLUENT. This RANS flowfield is used for calculating jet noise. The same procedure is repeated for each case of the parametric study. In the present study, the microjet angle is varied from 45 to 90<sup>0</sup> and the total injected mass flow rate is varied from 0.0036 to 0.0108 of the main jet mass flow rate. The number, diameter and Mach number of the microjets is kept constant for this study. Figure 28 shows that there is a minor effect of microjet angle on jet noise. The jet noise reduction is mainly observed at low frequencies. Figure 29 shows that the jet noise reduction is achieved up to a certain injected mass flow rate (i.e.  $R_m$  is the ratio of the injected mass flow rate per microjet to the main jet mass flow rate = 0.0004, therefore the total injected mass flow rate = 0.0072 of the main jet mass flow rate) and then the impact of microjets on jet noise deteriorates with further increase of the injected mass flow rate. This shows that a small amount of the injected mass flow can considerably reduce jet noise.

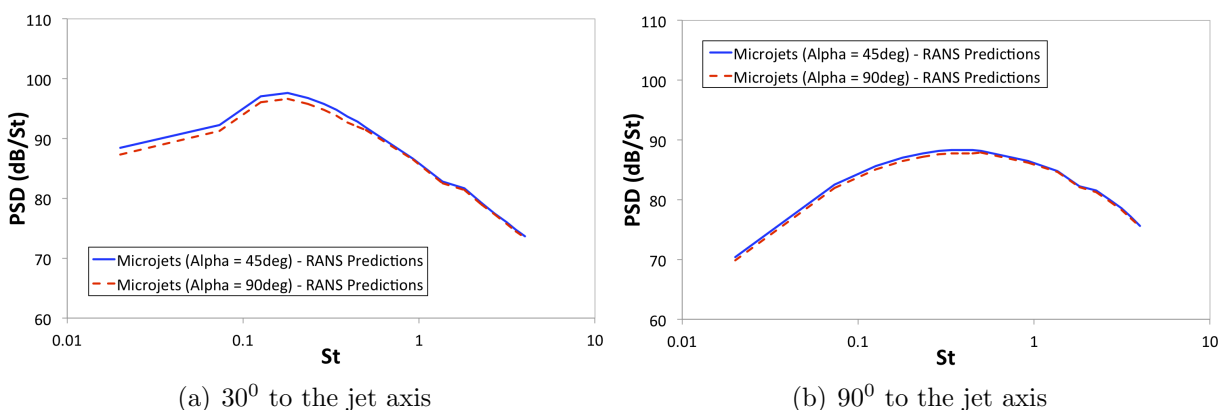


Figure 28. Effect of the microjet angle on jet noise

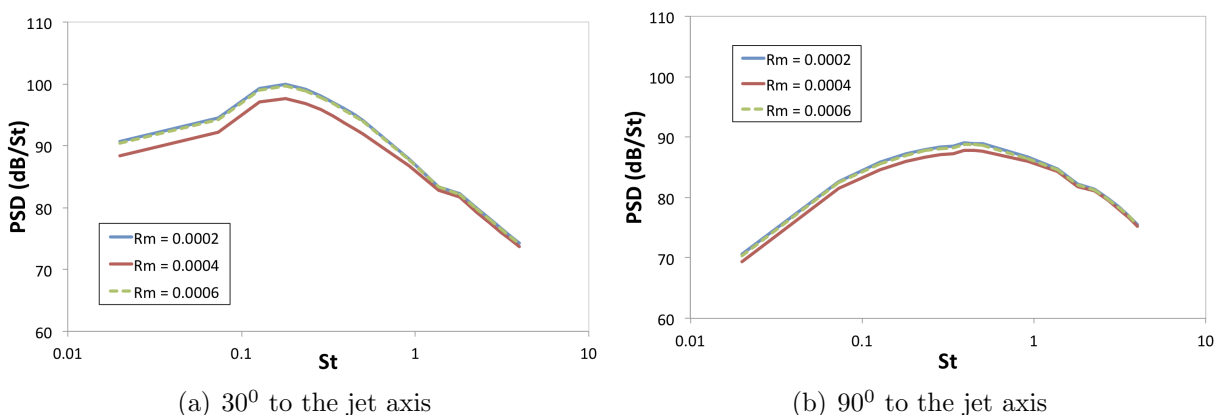


Figure 29. Effect of the injected mass flow rate on jet noise

## V. Conclusions

We know from our previous study (Depuru Mohan *et al.*<sup>18</sup>) that the  $R_{1111}$  is the dominant cross-correlation in the noise sources of unheated jets. Other major cross-correlations are  $R_{2222}$ ,  $R_{3333}$ ,  $R_{1212}$ ,  $R_{1313}$ ,  $R_{2323}$  and the cross-correlations equal to them by symmetry. We found that RANS is able to capture the variation of the scales that describe these sources with position within the jet and that there is a proportionality between turbulence scales that are taken from RANS and acoustic source scales that was validated through comparison with a LES flowfield. The proportionality constants were determined by curve fitting RANS scales on to LES scales and were found to be independent of source location and nozzle geometry. The acoustic sources are then described by these derived RANS scales. There was a good agreement between jet noise predictions and measurements over a wide range of frequencies and observer angles. However, in our previous work the relative amplitudes of  $R_{ijkl}(\mathbf{y}, \mathbf{0}, 0)$  cross-correlations with respect to the  $R_{1111}(\mathbf{y}, \mathbf{0}, 0)$  cross-correlation were taken from LES.

In the present study, a novel equation is proposed to express the amplitude of the fourth-order space-time cross-correlations in terms of mean flow parameters and turbulence statistics that can be obtained from RANS. The ratio of the amplitude of these cross-correlations to the square of turbulent kinetic energy is constant for a round jet. The same is true for the  $R_{1111}$  cross-correlation for a chevron jet but for  $R_{2222}$  and  $R_{3333}$  cross-correlations the ratio decreases up to four jet diameters downstream and then it becomes roughly constant and equal to the round jet level. For a chevron jet,  $R_{2222}$  and  $R_{3333}$  cross-correlations have an additional term proportional to the streamwise circulation which varies with axial distance. Noting this enabled us to propose an equation for the amplitude of the fourth-order space-time cross-correlations. The proposed equation is the sum of two terms; the first one is proportional to the square of turbulent kinetic energy and the second one is a combination of streamwise circulation, local turbulent kinetic energy and local mean axial velocity. This equation involves two non-dimensional constants,  $\alpha_{ijkl}$  and  $\beta_{ijkl}$ .  $\alpha_{ijkl}$  is defined as the ratio of the amplitude of a cross-correlation to the square of the turbulent kinetic energy and is based on analysis of a round jet.  $\beta_{ijkl}$  was found by curve-fitting to the LES results of the chevron jet. It was found that  $\alpha_{ijkl} = 0.7$  for  $R_{1111}$ ; 0.27 for  $R_{2222}$  and  $R_{3333}$ ; 0.23 for  $R_{1212}$  and  $R_{1313}$ ; 0.14 for  $R_{2323}$ ;  $\beta_{ijkl} = 0$  for  $R_{1111}$  and 0.07 for the other cross-correlations. The cross-correlations based on this model and a RANS flowfield showed a good agreement throughout the jet with those determined from a LES flowfield. This demonstrates that the proposed equation provides an accurate description of cross-correlations based completely on RANS once the constants of proportionality have been determined. The novel equation rather implies that there is a direct link between the mean jet flow and turbulence statistics

and the acoustic sources. With this source description, there is a good agreement between the model's jet noise predictions and measurements for a wide range of frequencies and observer angles for chevron jets.

As the model provides quick and accurate noise predictions for unheated jets, a parametric study was performed to investigate the impact of chevrons on jet noise. There is a significant jet noise reduction with the increase of chevron angle. However, aggressive chevron angles resulted in major thrust loss. Initially there is a rapid reduction in jet noise from a round nozzle as the chevron angle is increased from zero. Then when the chevron angle is increased beyond a critical value, the marginal increase in noise reduction decreases. The same is observed when chevron length is increased. Chevron penetration is found to be the underpinning factor for jet noise reduction. The jet noise reduction is comparable for chevron nozzles that have the same number of chevrons and the same penetration. There is a considerable jet noise reduction up to a chevron count of six and then the effect of chevrons decreases with a further increase in chevron count. The jet noise reduction by chevrons is more significant at  $30^\circ$  to the jet flow compared to  $90^\circ$ . Initially the reduction of jet noise per unit thrust loss is constant with increasing chevron penetration. Once the chevron penetration exceeds one-seventh of the nozzle diameter, the thrust loss increases more rapidly. The predicted and measured optimum values match very well for chevron jets.

With the novel source description and same proportionality constants as that of chevron and round jets, there is an excellent agreement between the model's jet noise predictions and measurements for a wide range of frequencies and observer angles for microjets. As the model provides quick and accurate jet noise predictions, a parametric study was performed to investigate the impact of microjets on jet noise. The number, diameter and Mach number of the microjets is kept constant for this study. The microjets were taken to have the same Mach number as the main jet. The injected mass flow rate has a major effect whereas, the microjet angle has a minor effect on jet noise. The optimum value of the injected mass flow rate per microjet is found to be around 0.0004 of the main jet mass flow rate i.e. the ratio of the total injected mass flow rate to the main jet flow rate is 0.0072. This shows that a small amount of the injected mass flow has a noticeable impact on jet noise. The predicted and measured optimum values match very well for microjets.

To conclude, a jet noise prediction model, which is developed and established for chevron jets, has also been validated for microjets. The model is indeed capable of assessing and optimising advanced jet noise reduction concepts and could contribute towards the development of quieter exhaust nozzles for future civil aircraft.

## Acknowledgments

Dr Depuru Mohan expresses his gratitude to St John’s College, University of Cambridge, for the award of a Dr Manmohan Singh Scholarship and Cambridge Commonwealth, European and International Trust for the award of a Cambridge International Scholarship. Authors are grateful to Dr Hynes (University of Cambridge); Dr Karabasov (Queen Mary, University of London) and Dr Graham (GE Global Research) for their initial support. Authors would like to specially thank Dr Xia (Loughborough University) and Professor Tucker (University of Cambridge) for providing the LES flow data for chevron and round jets.

## References

- <sup>1</sup>Bridges, J. E. and Brown, C. A., “Parametric testing of chevrons on single flow hot jets,” *NASA Technical Report*, 2004, pp. 1–17.
- <sup>2</sup>Callender, B., Gutmark, E., and Martens, S., “Far-field acoustic investigation into chevron nozzle mechanisms and trends,” *AIAA Journal*, Vol. 43, No. 1, 2005, pp. 87–95.
- <sup>3</sup>Callender, B., Gutmark, E., and Martens, S., “Near-field investigation of chevron nozzle mechanisms,” *AIAA Journal*, Vol. 46, No. 1, 2008, pp. 36–45.
- <sup>4</sup>Arakeri, V. H., Krothapalli, A., Siddavaram, V., Alkislar, M. B., and Lourenco, L. M., “On the use of microjets to suppress turbulence in a Mach 0.9 axisymmetric jet,” *Journal of Fluid Mechanics*, Vol. 490, No. 1, 2003, pp. 75–98.
- <sup>5</sup>Castelain, T., Sunyach, M., Juvé, D., and Bera, J.-C., “Jet-noise reduction by impinging microjets: an acoustic investigation testing microjet parameters,” *AIAA journal*, Vol. 46, No. 5, 2008, pp. 1081–1087.
- <sup>6</sup>Zaman, K. B. M. Q., “Subsonic jet noise reduction by microjets – a parametric study,” *International Journal of Aeroacoustics*, Vol. 9, No. 6, 2010, pp. 705–732.
- <sup>7</sup>Henderson, B., “Fifty years of fluidic injection for jet noise reduction,” *International Journal of Aeroacoustics*, Vol. 9, No. 1, 2010, pp. 91–122.
- <sup>8</sup>Xia, H., Karabasov, S. A., Graham, O., Tucker, P. G., Dowling, A. P., Depuru Mohan, N. K., and Hynes, T. P., “Hybrid RANS–LES modeling of chevron nozzles with prediction of far field sound,” *AIAA Aerospace Sciences Meeting*, 2011.
- <sup>9</sup>Ffowcs Williams, J. E. and Hawkins, D. L., “Sound generation by turbulence and surfaces in arbitrary motion,” *Philosophical Transactions of the Royal Society of London. Series A, Mathematical and Physical Sciences*, Vol. 264, 1969, pp. 321–342.
- <sup>10</sup>Karabasov, S. A., Afsar, M. Z., Hynes, T. P., Dowling, A. P., McMullan, W. A., Pokora, C. D., Page, G. J., and McGuirk, J. J., “Jet noise: acoustic analogy informed by large eddy simulation,” *AIAA Journal*, Vol. 48, No. 7, 2010, pp. 1312–1325.
- <sup>11</sup>Bodony, D. and Lele, S. K., “Current status of jet noise predictions using large-eddy simulation,” *AIAA Journal*, Vol. 46, 2005, pp. 364–380.
- <sup>12</sup>Engel, R., Silva, C., and Deschamps, C., “Application of RANS-based method to predict acoustic noise of chevron nozzles,” *Applied Acoustics*, Vol. 79, 2014, pp. 153–163.

- <sup>13</sup>Enomoto, S., Yamamoto, K., Yamashita, K., Tanaka, N., Oba, Y., and Oishi, T., “Large-eddy simulation of high-subsonic jet flow with microjet injection,” *17th AIAA/CEAS Aeroacoustics Conference*, 2011.
- <sup>14</sup>Laurendeau, E., Jordan, P., Bonnet, J. P., Delville, J., Parnaudeau, P., and Lamballais, E., “Subsonic jet noise reduction by fluidic control: The interaction region and the global effect,” *Physics of Fluids*, Vol. 20, 2008, pp. 1015–19.
- <sup>15</sup>Najafi-Yazdi, A., Lew, P.-T., and Mongeau, L., “Large eddy simulation of jet noise suppression by impinging microjets,” *17th AIAA/CEAS Aeroacoustics Conference*, Vol. 2748, 2011.
- <sup>16</sup>Rife, M. E. and Page, G. J., “Large eddy simulation of high Reynolds number jets with microjet injection,” *17th AIAA/CEAS Aeroacoustics Conference*, Vol. 2882, 2011.
- <sup>17</sup>Shur, M. L., Spalart, P. R., and Strelets, M. K., “LES-based evaluation of a microjet noise reduction concept in static and flight conditions,” *Journal of Sound and Vibration*, Vol. 330, No. 17, 2011, pp. 4083–4097.
- <sup>18</sup>Depuru Mohan, N. K., Dowling, A. P., Karabasov, S. A., Xia, H., Graham, O., Hynes, T. P., and Tucker, P. G., “Acoustic sources and far-field noise of chevron and round jets,” *AIAA Journal*, Vol. 53, No. 9, 2015, pp. 2421–2436.
- <sup>19</sup>Spalart, P. and Allmaras, S., “A one-equation turbulence model for aerodynamic flows,” *La Recherche Aeronautique*, Vol. 1, 1994, pp. 5–21.
- <sup>20</sup>Xia, H. and Tucker, P. G., “Numerical simulation of single-stream jets from a serrated nozzle,” *Flow, Turbulence and Combustion*, Vol. 88, 2012, pp. 3–18.
- <sup>21</sup>Xia, H., Tucker, P. G., and Eastwood, S., “Large-eddy simulations of chevron jet flows with noise predictions,” *International Journal of Heat and Fluid Flow*, Vol. 30, No. 6, 2009, pp. 1067–1079.
- <sup>22</sup>Tam, C. K. W. and Auriault, L., “Mean flow refraction effects on sound radiated from localized sources in a jet,” *Journal of Fluid Mechanics*, Vol. 370, No. 2, 1998, pp. 149–174.